Math Geosci (2015) 47:471–495
DOI 10.1007/s11004-014-9556-8

Joint Simulation of Grade and Rock Type in a Stratabound Copper Deposit

Mohammad Maleki · Xavier Emery

Received: 23 December 2013 / Accepted: 18 August 2014 / Published online: 5 September 2014

Abstract This work deals with the joint simulation of copper grade (as a continuous regionalized variable) and rock type (as a categorical variable) in Lince–Estefanía deposit, located in northern Chile. The region under study is heterogeneous, containing three main rock types (intrusive, andesite and breccia bodies) with different copper grade distributions. To perform joint simulation, the multi-Gaussian and pluri-Gaussian models are used in a combined form. To this end, three auxiliary Gaussian random fields are considered, one for simulating copper grade, up to a monotonic transformation, and two for simulating rock types according to a given truncation rule. Furthermore, the dependence between copper grade and rock types is reproduced by considering cross correlations between these Gaussian random fields. To investigate the benefits of the joint simulation algorithm, copper grade and rock types are also simulated by the traditional cascade approach and the results are compared. It is shown that the cascade approach produces hard boundaries, that is, abrupt transitions of copper grades when crossing rock-type boundaries, a condition that does not exist in the study area according to the contact analysis held on the available data. In contrast, the joint simulation approach produces gradual transitions of the copper grade near the rock-type boundaries and is more suited to the actual data.

M. Maleki · X. Emery (✉)
Department of Mining Engineering, University of Chile, Santiago, Chile
e-mail: xemery@ing.uchile.cl

M. Maleki · X. Emery
Advanced Mining Technology Center, University of Chile, Santiago, Chile
e-mail: mohammad.maleki@ing.uchile.cl

M. Maleki
CSIRO-Chile International Center of Excellence
in Mining and Mineral Processing, Santiago, Chile

Keywords Contact analysis · Multi-Gaussian model · PluriGaussian model · Joint modeling · Geological heterogeneity

1 Introduction

In ore body modeling, it is often of interest to assess the spatial variability of geological parameters such as rock types and grades of elements of interest, which is a key factor in downstream processes, such as mine planning and management, and provides information on geological heterogeneity at multiple scales. Because the spatial distributions of grades and rock types are often interdependent, a separate modeling of these two parameters is inadequate. Instead, it is more natural to consider a joint modeling of grades and rock types. Nowadays, a hierarchical approach (or cascade approach) is usually applied for this purpose. It means that, first of all, the layout of each rock type is delimited in the study area. In this respect, one can use a deterministic model based on geological knowledge and available exploration data (Duke and Hanna 2001; Mackenzie and Wilson 2001), or a stochastic model based on simulating the occurrence of each rock type in the study area (Journel and Alabert 1990; Armstrong et al. 2011; Chilès and Delfiner 2012; Strebelle 2002, to name a few). After delimitating the rock-type layouts, the grades are simulated in each rock type separately using only the data that belong to this rock type, leading to a piecewise grade model (Alabert and Massonnat 1990; Roldão et al. 2012; Boucher and Dimitrakopoulos 2012; Jones et al. 2013). Although this cascade approach is simple, it has some substantial drawbacks. For instance, it does not take into account the dependence between the grades across rock-type boundaries; therefore, except for the case of a hard boundary for which there exists a sudden change in the grade distribution when crossing the boundary (Kim et al. 2005), it does not properly reflect the spatial relationship between the grades and the occurrence of given rock types (Wilde and Deutsch 2012; Rossi and Deutsch 2014). In addition, when using a deterministic rock-type model, one works with a single interpretation of the deposit and does not account for any uncertainty in the rock-type layout.

To account for the spatial dependence of grade across rock-type boundaries, Larrondo et al. (2004) and Ortiz and Emery (2006) suggest modeling not only the direct, but also the cross-correlation functions of the grades variables defined separately within each rock type, while Vargas-Guzman (2008) proposes a stepwise modeling of these grade variables using successive conditional covariance functions. In all cases, a piecewise grade model is still considered, insofar as the grade is split into as many variables as rock types, which does not allow for smooth transitions across rock types. An alternative approach that avoids such a piecewise modeling is to jointly simulate the grades and rock types. This approach is more complex because of the different natures of these two parameters: grades are measured on a continuous quantitative scale, whereas rock types are measured on a nominal scale. To overcome this difficulty, one can integrate two well-known geostatistical models, as proposed by Emery and Silva (2009) and Cáceres and Emery (2010): the multi-Gaussian model for simulating grades and the truncated pluriGaussian model for simulating rock types. This approach allows a flexible modeling of the contact relationships between rock

types and the dependence relationships between grades and rock types, but, to the best of the authors' knowledge, so far it has been applied only to disseminated deposits.

The objective of this paper is to apply the joint simulation approach to a stratabound copper deposit, to quantify the uncertainty in the copper grades and prevailing rock types, and to compare this approach with the aforementioned cascade approach. The outline is as follows: after a brief recall on the methodology, the case study will be presented, consisting of exploratory data analysis, contact analysis, joint modeling of grade and rock type, joint simulation and analysis of results.

2 Methodology

2.1 Multi-Gaussian Simulation of Grades

The multi-Gaussian model is widespread for simulating mineral grades (Journel and Huijbregts 1978). The implementation consists of the following steps. First, one has to transform the grade data into normal scores and fit a variogram to the transformed data. Then, a Gaussian random field is simulated by use of algorithms such as the turning bands, sequential or spectral simulation (Deutsch and Journel 1998; Lantuéjoul 2002; Chilès and Delfiner 2012). Finally, the simulated Gaussian values are back transformed to grade values.

2.2 PluriGaussian Simulation of Rock Types

PluriGaussian simulation aims at constructing realizations of a categorical variable (a rock type in the present case), represented by the truncation of one or more Gaussian random fields. First, according to the spatial relationships and contacts between rock types, one has to define a number of Gaussian random fields and a truncation rule (Lantuéjoul 2002; Dowd et al. 2003; Armstrong et al. 2011). Afterwards, the spatial correlation structure of the Gaussian random fields is modeled, to fit the rock-type indicator variograms. With respect to simulation, a set of Gaussian values are first generated at the data locations, conditionally to the rock-type data, by Gibbs sampling. Then, multi-Gaussian simulation is performed over the study area. Finally, using the truncation rule, the simulated Gaussian values are converted into rock types.

2.3 Joint Simulation of Grade and Rock Type

The joint simulation approach uses the multi-Gaussian model to simulate the grades and the pluriGaussian model to simulate the rock types. The novelty is that the underlying Gaussian random fields are supposed to be spatially cross-correlated, which allows introducing a spatial dependence between rock types and grades. When all the Gaussian random fields have been jointly simulated, using the back-transformation and truncation rule, one can obtain the simulated grades and rock types. Details of the approach can be found in Emery and Silva (2009). Figure 1 illustrates the main steps of the approach.

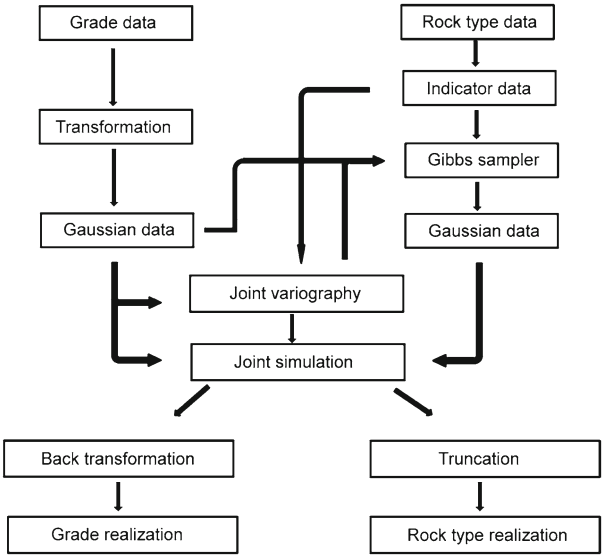

Fig. 1 Steps of joint simulation approach

3 Case Study: Lince–Estefanía Deposit

The case study under consideration corresponds to a stratabound manto-type copper deposit located in northern Chile and operated by Minera Michilla. Mining is achieved through underground (Estefanía) and open pit (Lince) operations.

3.1 Geological Description

The Lince–Estefanía deposit Michilla is located 130 km north–northeast of Antofagasta city, Chile. The host sequence comprises andesitic basaltic lava flows of the La Negra Formation (Oliveros et al. 2008). This sequence has been intruded by diorite to granite bodies, dykes, as well as breccia bodies with volcanic clasts and an intrusive matrix. Breccia bodies are generally located around the dioritic intrusions and extend laterally from the intrusions into stratabound manto bodies. Breccias with high copper content are believed to be pre- or syn-mineralization. The main ore minerals are copper oxides (predominantly atacamite and chrysocolla), which dominate near the surface (above 500 m a.m.s.l.), and copper sulfides (chalcocite, bornite, covellite and chalcopyrite), which dominate at elevations below 250 m a.m.s.l. From 250 to 500 m a.m.s.l., a mixed sulfide-oxide transition is found. Chemical analyses of the ores, as well as field and petrographic observations, indicate that copper sulfides in stratabound-manto and breccia ore bodies were formed by the same processes, which suggests that one may observe a correlation of copper grades across these rock types.

3.2 Presentation of the Data Set

The case study will be developed on the basis of an exploration data set from diamond and reversed-circulation drill holes. For the sake of simplicity, the data have been restricted to a small portion of the deposit and the grade values have been multiplied by a constant factor to preserve data confidentiality. Concerning rock types, three main types will be considered for modeling:

- *Intrusive bodies* (*code 1*), consisting of dioritic bodies with thicknesses from 20 to 450 m, associated with small dykes that crosscut all the other rock types. Their boundary with the surrounding rocks is irregular.
- *Andesite* (*code 2*), composed of aphanitic andesites, porphyritic andesites, ocoites and metandesites that are unlikely to contain economic copper mineralization due to their low permeability. It is widely distributed in the deposit, with a monoclinal structure that strikes at N65°E and dips at 35–40°NW, and is part of the volcanic sequence known as La Negra Formation.
- *Volcanic breccias bodies* (*code 3*), composed of amygdaloidal andesites and volcanic breccias that are likely to hold copper mineralization due to their high porosity. As for andesites, it is part of the La Negra Formation. It extends into stratabound manto bodies and occupies a monoclinal structure that strikes at N65°E and dips at 35–40°NW.

A cross section showing the data is presented in Fig. 2, which uses local coordinates (abscissa axis oriented along the direction N65°E). A summary of descriptive statistics and a visualization of the copper grade distribution is given in Table 1 and Fig. 3, showing a dependence between grade and rock type, with volcanic breccias (rock type 3) having the highest average copper grade and intrusive bodies (rock type 1)

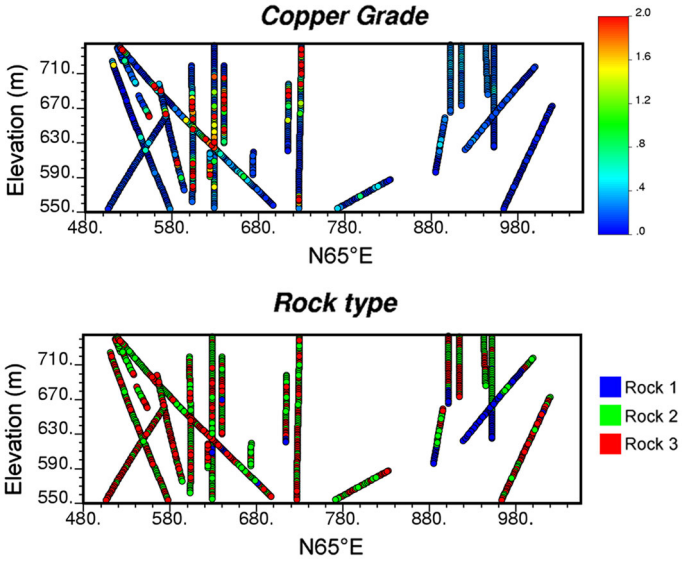

Fig. 2 Location of copper grade and rock-type data over a cross section of the deposit

Table 1 Statistics of grade data (in %), globally and per rock type

	Global	Rock type 1	Rock type 2	Rock type 3
Count	7,173	619	3,680	2,874
Minimum	0.00	0.00	0.00	0.00
Maximum	17.07	2.38	14.51	17.07
Mean	0.49	0.136	0.352	0.746
Standard deviation	1.14	0.187	0.709	1.576
Median	0.18	0.09	0.18	0.20

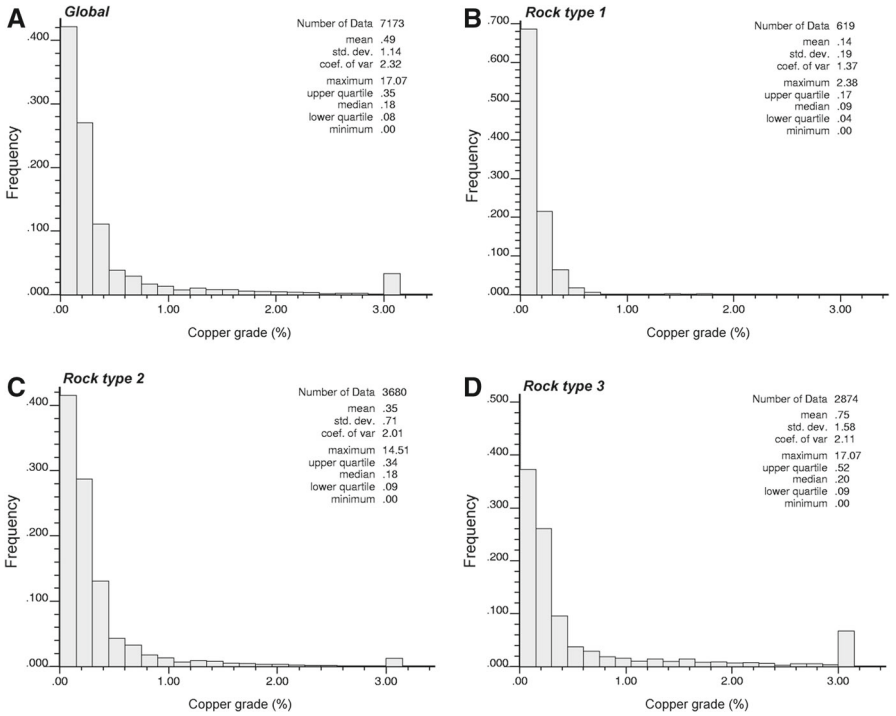

Fig. 3 Histograms of copper grade data, overall (**a**) and per rock type (**b**, **c**, **d**)

the lowest average copper grade. To better understand the dependence relationships between grade and rock type, a contact analysis is performed next.

3.3 Contact Analysis

The analysis aims at determining the behavior of the copper grade in the neighborhood of the boundary between two rock types (Glacken and Snowden 2001; Wilde and Deutsch 2012). In practice, two kinds of analysis can be performed. The first one is a mean value contact analysis, consisting in grouping the data of one rock type into classes of distance from the boundary with another rock type (as an approximation, one often considers the distance to the closest data of this second rock type in the same

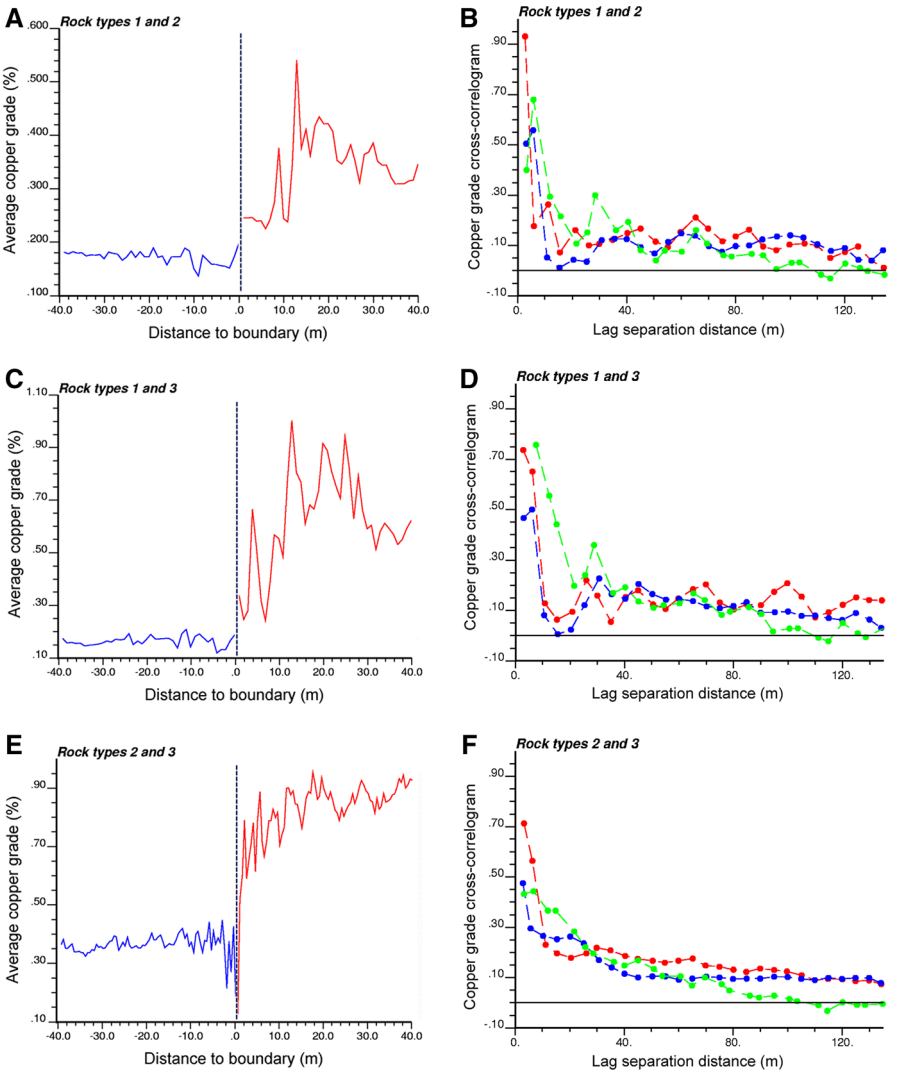

Fig. 4 Contact analysis between rock types: **a**, **c**, **e** mean grade graphs; **b**, **d**, **f** cross-correlation functions calculated along main anisotropy directions (*green* N25°W, *red* N115°E dip −60°, *blue* N25°W dip −30°)

drill hole), then plotting the mean grade of each group as a function of the distance to the boundary (Rossi and Deutsch 2014). The resulting plot shows how the mean grade varies when getting closer or farther to a boundary. The second analysis is a cross-correlation contact analysis, which consists in identifying pairs of data with a given lag separation distance that belong to two different rock types and plotting the correlation coefficient between such data pairs as a function of the lag separation distance. The plot indicates how much correlated are the grade values between both sides of the boundary. As a result, one observes a soft contact between all rock types, characterized by a rather smooth transition of the mean grade (Fig. 4a, c, e) and a

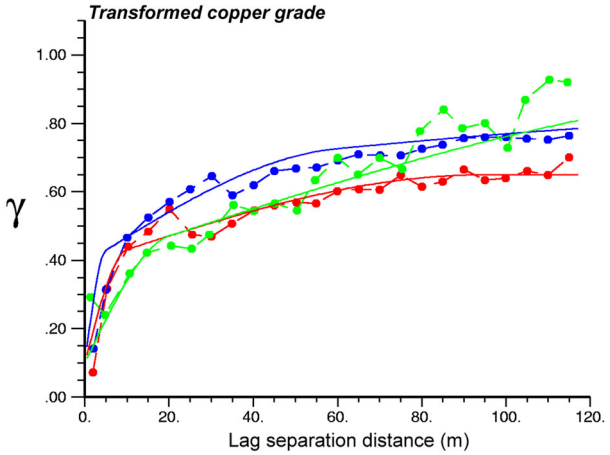

Fig. 5 Sample (*dashed lines*) and modeled (*solid lines*) variograms of normal scores data associated with grade, calculated along main anisotropy directions (*green* N25°W, *red* N115°E dip −60°, *blue* N25°W dip −30°)

correlation that does not vanish at small lag separation distances (Fig. 4b, d, f). The width of the transition zone is limited to 10 to 20 m, which makes a difference between this deposit (a high-variability stratabound deposit) and disseminated porphyry copper deposits with thicker transition zones.

3.4 Copper Grade Modeling

The grade data are transformed into normal scores (associated with a Gaussian random field Y_0) prior to performing variogram analysis. The modeled variogram (denoted as g_{00}) consists of a nugget effect and four nested anisotropic spherical structures (Fig. 5)

$$\begin{aligned} g_{00} = {} & 0.1\text{nugget} + 0.29\text{sph}(20, 10, 5) + 0.26\text{sph}(175, 95, 60) \\ & + 0.17\text{sph}(195, \infty, 195) + 0.18\text{sph}(500, \infty, \infty). \end{aligned} \quad (1)$$

In the above formula, the distances into brackets indicate the ranges (expressed in meters) along the main anisotropy directions.

3.5 Rock-Type Modeling

3.5.1 Truncation Rule

The examination of the drill hole data indicates that all the rock types are in contact. If one considers two independent Gaussian random fields (Y_1 and Y_2) for pluriGaussian simulation, then three simple truncation rules can be considered to reproduce the contacts between rock types (Fig. 6). To determine which of these truncation rules is best suited to the data, a simple way is to examine the direct and cross variograms of

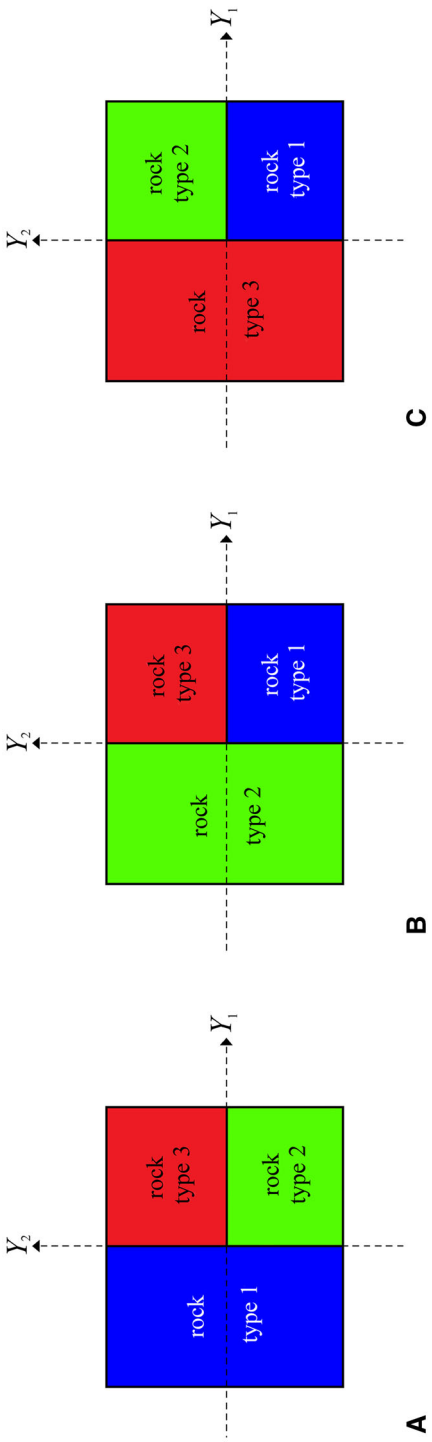

Fig. 6 Possible truncation rules for pluriGaussian modeling

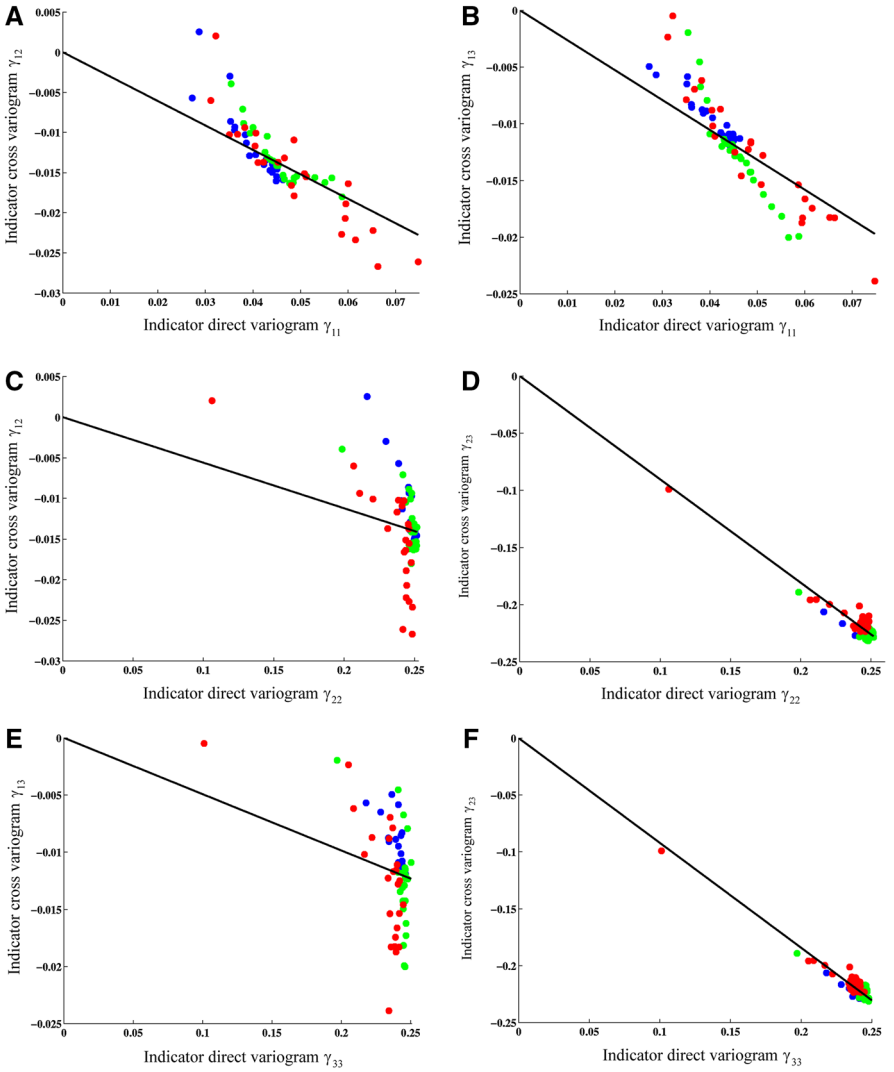

Fig. 7 Cross versus direct variograms of rock-type indicators, calculated along main anisotropy directions (*green* N25°W, *red* N115°E dip −60°, *blue* N25°W dip −30°). *Straight lines* indicating perfect proportionality are superimposed

rock-type indicators. More specifically, if γ_{ij} represents the cross variogram between the indicators of rock types i and j, then (proof in Appendix A)

- $\frac{\gamma_{12}}{\gamma_{11}}$ and $\frac{\gamma_{13}}{\gamma_{11}}$ do not vary with the lag separation vector in the model of Fig. 6a
- $\frac{\gamma_{12}}{\gamma_{22}}$ and $\frac{\gamma_{23}}{\gamma_{22}}$ do not vary with the lag separation vector in the model of Fig. 6b
- $\frac{\gamma_{13}}{\gamma_{33}}$ and $\frac{\gamma_{23}}{\gamma_{33}}$ do not vary with the lag separation vector in the model of Fig. 6c.

Experimentally, one observes that γ_{12} and γ_{13} are practically proportional to γ_{11} (Fig. 7a, b), but not to γ_{22} (Fig. 7c) or γ_{33} (Fig. 7e). Accordingly, the ratios γ_{12}/γ_{11}

and γ_{13}/γ_{11} can be considered as independent of the lag separation vector, whereas the ratios γ_{12}/γ_{22} and γ_{13}/γ_{33} cannot. This suggests that Fig. 6a is the best truncation rule to describe the contact relationships between rock types. Such a truncation rule, in which rock type 1 (intrusive bodies) appears to crosscut the other two rock types, furthermore agrees with the geology of the deposit, insofar as rock type 1 is the youngest one (dated between 168 and 112 Ma) and intruded both andesite and breccia bodies, which pertain to the Jurassic La Negra Formation (Oliveros et al. 2008).

The truncation rule will therefore be defined on the basis of two thresholds, associated with two independent Gaussian random fields Y_1 and Y_2, as follows:

- Location $\mathbf{x}$ belongs to rock type 1 if $Y_1(\mathbf{x}) \leq y_1$
- Location $\mathbf{x}$ belongs to rock type 2 if $Y_1(\mathbf{x}) > y_1$ and $Y_2(\mathbf{x}) \leq y_2$
- Location $\mathbf{x}$ belongs to rock type 3 if $Y_1(\mathbf{x}) > y_1$ and $Y_2(\mathbf{x}) > y_2$.

The truncation thresholds y_1 and y_2 can be defined according to the rock-type proportions (Armstrong et al. 2011). This leads to the following threshold values: $y_1 = -1.405$ and $y_2 = 0.137$.

3.5.2 Variogram Analysis

To complete the pluriGaussian model, it remains to fit the variograms of the two underlying Gaussian random fields Y_1 and Y_2. Because these random fields are assumed independent, their cross variogram is zero. As for the direct variograms, a trial-and-error procedure is used, to fit the variograms of rock-type indicators (Emery 2007; Emery and Silva 2009). At this stage, an important practical aspect to consider is that, in the following section, we will be interested in cross-correlating the two Gaussian random fields used in the pluriGaussian model with the Gaussian random field already used in the multi-Gaussian model [Eq. (1)]. Therefore, it is advisable to consider all or part of the basic nested structures used for grade modeling (Sect. 3.4). Following this recommendation, the variograms of Gaussian random fields associated with the pluriGaussian model (denoted by g_{11} and g_{22}) are found to be

$$\begin{aligned} g_{11} &= 0.07\text{sph}(20, 10, 5) + 0.161\text{sph}(175, 95, 60) \\ &\quad + 0.197\text{sph}(195, \infty, 195) + 0.572\text{sph}(500, \infty, \infty) \qquad (2) \\ g_{22} &= 0.50\text{sph}(20, 10, 5) + 0.50\text{sph}(30, 20, 10). \qquad (3) \end{aligned}$$

In these formulae, the distances into brackets indicate the ranges along the same directions as for the grade data. The sample and modeled indicator direct and cross variograms are shown in Fig. 8. The cross variograms are negative due to the compositional nature of the rock-type indicators: the increase of an indicator (from 0 to 1) is necessarily associated with the decrease of another indicator (from 1 to 0).

3.6 Modeling the Spatial Dependence Between Grade and Rock Type

Up to now, six nested structures (a nugget effect and five spherical structures) have been introduced. The first spherical structure is common for the Gaussian random

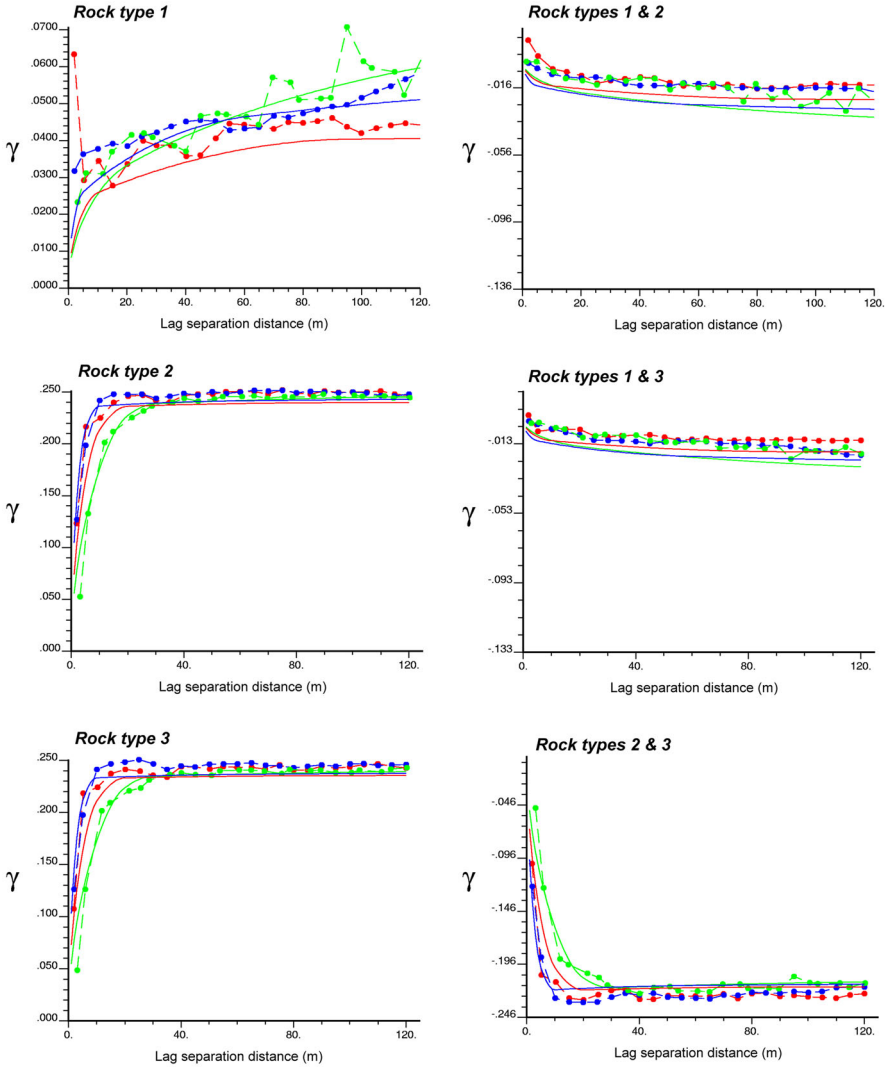

Fig. 8 Sample (*dashed lines*) and modeled (*solid lines*) direct and cross variograms of indicator data associated with rock types, calculated along main anisotropy directions (*green* N25°W, *red* N115°E dip −60°, *blue* N25°W dip −30°)

fields associated with the grade (Y_0) and with the rock type (Y_1 and Y_2). The next three spherical models are common for Y_0 and Y_1, the last spherical model only pertains to Y_2, whereas the nugget effect only pertains to Y_0. To cross-correlate grade and rock type, we will now propose a linear model of coregionalization for Y_0, Y_1 and Y_2. From the previous steps, some entries of the coregionalization matrices associated with the aforementioned nested structures are already specified: the diagonal entries correspond to the direct variograms of Y_0, Y_1 and Y_2, while the off-diagonal entries between Y_1 and Y_2 are equal to zero because Y_1 and Y_2 are independent. Also, the entry

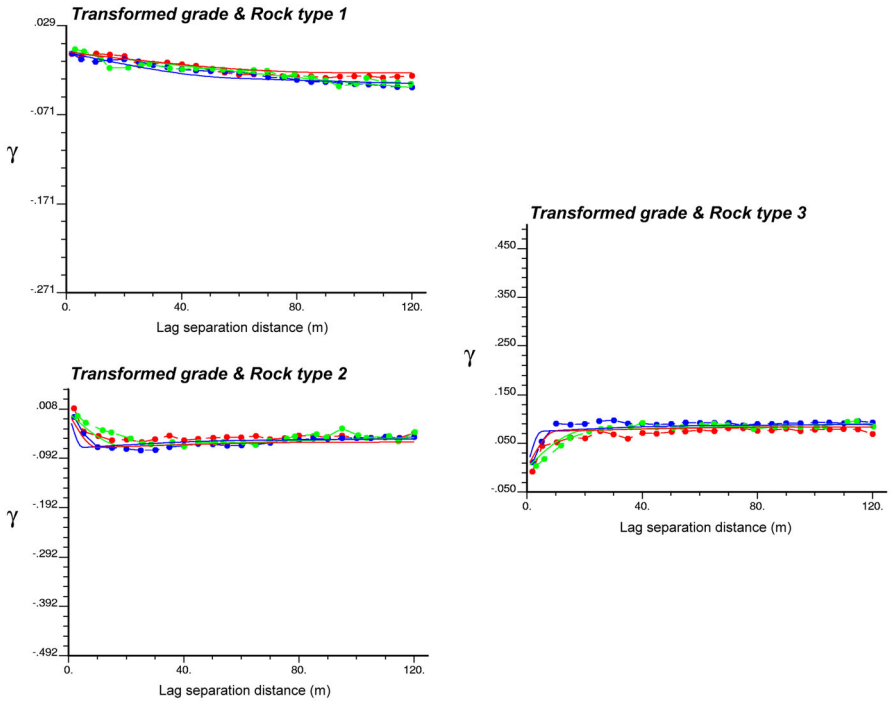

Fig. 9 Sample (*dashed lines*) and modeled (*solid lines*) cross variograms between indicators data and transformed grade data, calculated along main anisotropy directions (*green* N25°W, *red* N115°E dip −60°, *blue* N25°W dip −30°)

associated with a cross variogram g_{ij} between Y_i and Y_j (with $i, j = 0, 1$ or 2) is zero when the entry associated with the direct variogram g_{ii} or g_{jj} is zero (Wackernagel 2003). Accordingly, it only remains to determine four entries (a, b, c, d)

$$\begin{pmatrix} g_{00} & g_{01} & g_{02} \\ g_{01} & g_{11} & g_{12} \\ g_{02} & g_{12} & g_{22} \end{pmatrix} = \begin{pmatrix} 0.1 & 0 & 0 \\ 0 & 0 & 0 \\ 0 & 0 & 0 \end{pmatrix} \text{nugget} + \begin{pmatrix} 0.29 & a & b \\ a & 0.07 & 0 \\ b & 0 & 0.50 \end{pmatrix} \text{sph}(20, 10, 5)$$
$$+ \begin{pmatrix} 0.26 & c & 0 \\ c & 0.161 & 0 \\ 0 & 0 & 0 \end{pmatrix} \text{sph}(175, 95, 60) + \begin{pmatrix} 0.17 & d & 0 \\ d & 0.197 & 0 \\ 0 & 0 & 0 \end{pmatrix} \text{sph}(195, \infty, 195)$$
$$+ \begin{pmatrix} 0.18 & e & 0 \\ e & 0.572 & 0 \\ 0 & 0 & 0 \end{pmatrix} \text{sph}(500, \infty, \infty) + \begin{pmatrix} 0 & 0 & 0 \\ 0 & 0 & 0 \\ 0 & 0 & 0.50 \end{pmatrix} \text{sph}(30, 20, 10). \quad (4)$$

For the fitting, one has to be aware of which Gaussian random field is modeling each rock type. For instance, the indicator of rock-type 1 only depends on random field Y_1, while the indicators of rock types 2 and 3 depend on both random fields Y_1

and Y_2. Accordingly, the cross variogram between the transformed grade (Y_0) and the indicator of rock type 1 only depends on the cross variogram between Y_0 and Y_1, while the cross variograms between the transformed grade and the indicator of rock type 2 or rock type 3 also depend on the cross variogram between Y_0 and Y_2. Based on the previous statements, the unknown coefficients (a, c, d, e) are first chosen (by trial-and-error) to fit the cross variogram between the transformed grade and the indicator of rock type 1. Once done, the last coefficient (b) is chosen in order to fit the cross variograms between the transformed grade and the indicators of rock types 2 and 3. The following values represent the best coincidence between sample and modeled cross variograms (Fig. 9)

$$a = 0.01; \quad b = 0.2; \quad c = 0.15; \quad d = 0.1; \quad e = 0.15. \tag{5}$$

To ensure the mathematical consistency of the proposed coregionalization model, one can check that all the defined coregionalization matrices are positive semi-definite, that is, their eigenvalues are nonnegative (Wackernagel 2003).

3.7 Joint Simulation Results

Provided with the model fitted in Sects. 3.4–3.6, one can construct realizations of grade and rock type. Simulation first consists in simulating the Gaussian random fields Y_1 and Y_2 at the data locations, conditionally to the grade and rock-type data, for which an iterative algorithm (Gibbs sampler) is necessary. Then, one performs a joint multi-Gaussian simulation of Y_0, Y_1 and Y_2; this is done by decomposing these random fields into spatially non-correlated factors using coregionalization analysis

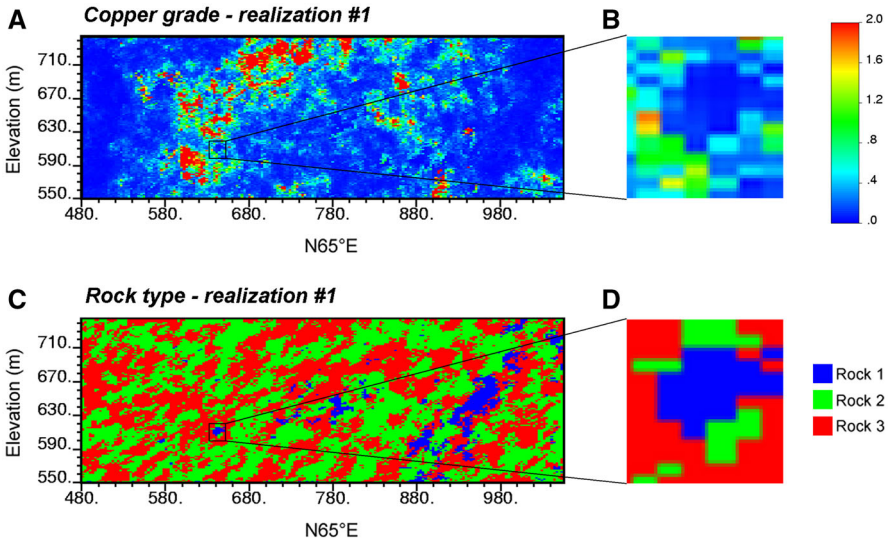

Fig. 10 One realization of copper grade and rock type (joint simulation)

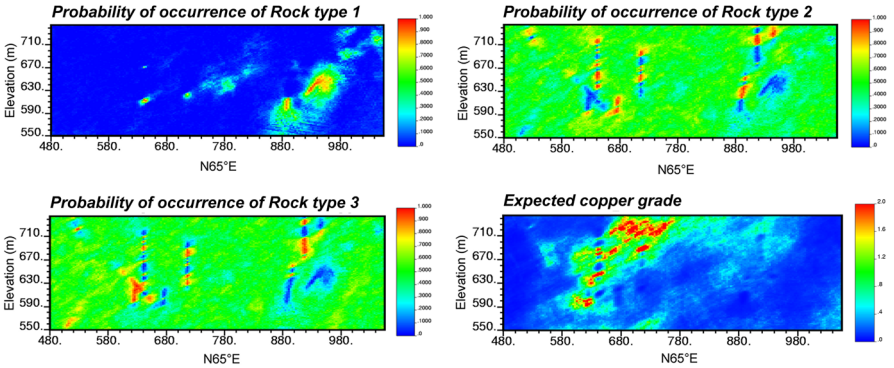

Fig. 11 Probabilities of occurrence of each rock type and expected copper grade, calculated over 100 realizations (joint simulation)

and by independently simulating the factors via the turning bands method (Emery 2008). Figure 10 shows one joint realization of grade and rock type over the same cross section as in Fig. 2, and Fig. 11 displays the probability of occurrence of each rock type and the expected copper grade calculated over 100 realizations. The drill hole locations are perceptible on the probability maps and correspond to the locations where the probability is close to zero or to one.

3.8 Cascade Simulation of Grade and Rock Type

The results of the joint simulation approach will now be compared to those of the more traditional cascade approach. The cascade approach consists in first simulating the layout of the rock types, then in simulating the copper grade in each rock type separately using only the data that belong to the rock type under consideration. The steps are the following.

1. For each rock type: transformation of the copper grade data into normal scores and variogram analysis of the normal scores data.
2. PluriGaussian simulation of each rock type, using the model presented in Sect. 3.5.
3. For each pluriGaussian realization and each rock type
   (a) Identify the nodes belonging to the rock type
   (b) Simulate copper grade conditionally to the grade data belonging to the rock type. At this stage, turning bands simulation is used (Emery and Lantuéjoul 2006).
4. Obtain copper grade realizations by juxtaposing the simulated grades in rock types 1, 2 and 3 (a single grade realization is associated with each rock type realization).

Figures 12 and 13 illustrate the results of the cascade simulation approach. The probability maps are similar to those obtained with the joint simulation approach, which is explained because the rock type is represented by the same pluriGaussian model in both approaches. In contrast, the map of expected copper grade shows stronger differences with the joint simulation approach, which can be observed by comparing Figs. 11 and 13.

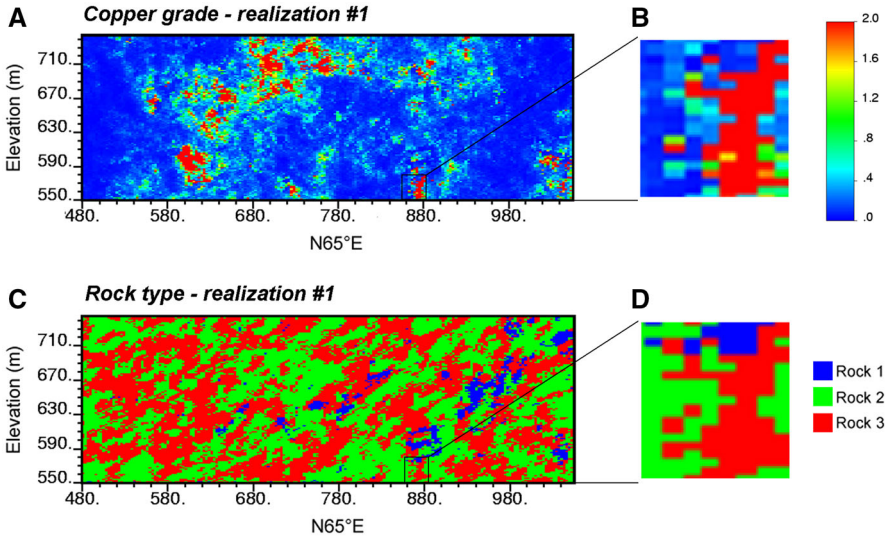

Fig. 12 One realization of copper grade and rock type (cascade simulation)

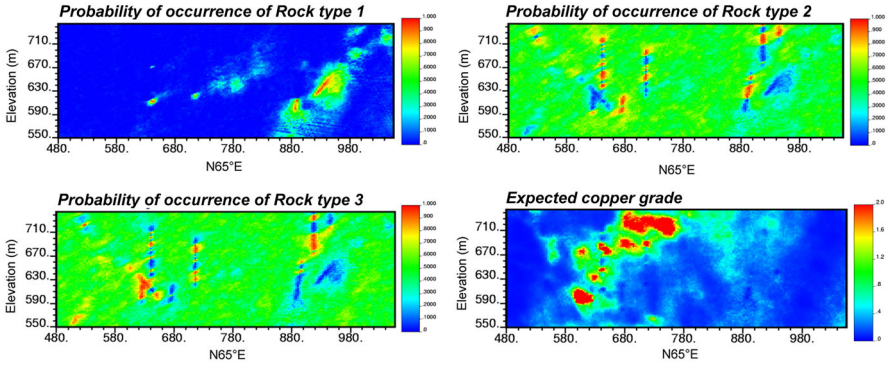

Fig. 13 Probabilities of occurrence of each rock type and expected copper grade, calculated over 100 realizations (cascade simulation)

3.9 Comparison of Results

3.9.1 Distribution of Copper Grade Conditioned to Rock Type

Since it accounts for cross correlations between grade and rock type through coefficients a, b, c, d and e in Eq. (4), the joint simulation model fitted in Sects. 3.4–3.6 yields a marginal grade distribution that differs from one rock type to another. Such a distribution of grade conditioned to the rock type can be assessed analytically using expansions into Hermite polynomials (Appendix B), or numerically by co-simulating the three Gaussian random fields (Y_0, Y_1, Y_2), converting the simulated Gaussian values into grades and rock types, and finally calculating the distributions of

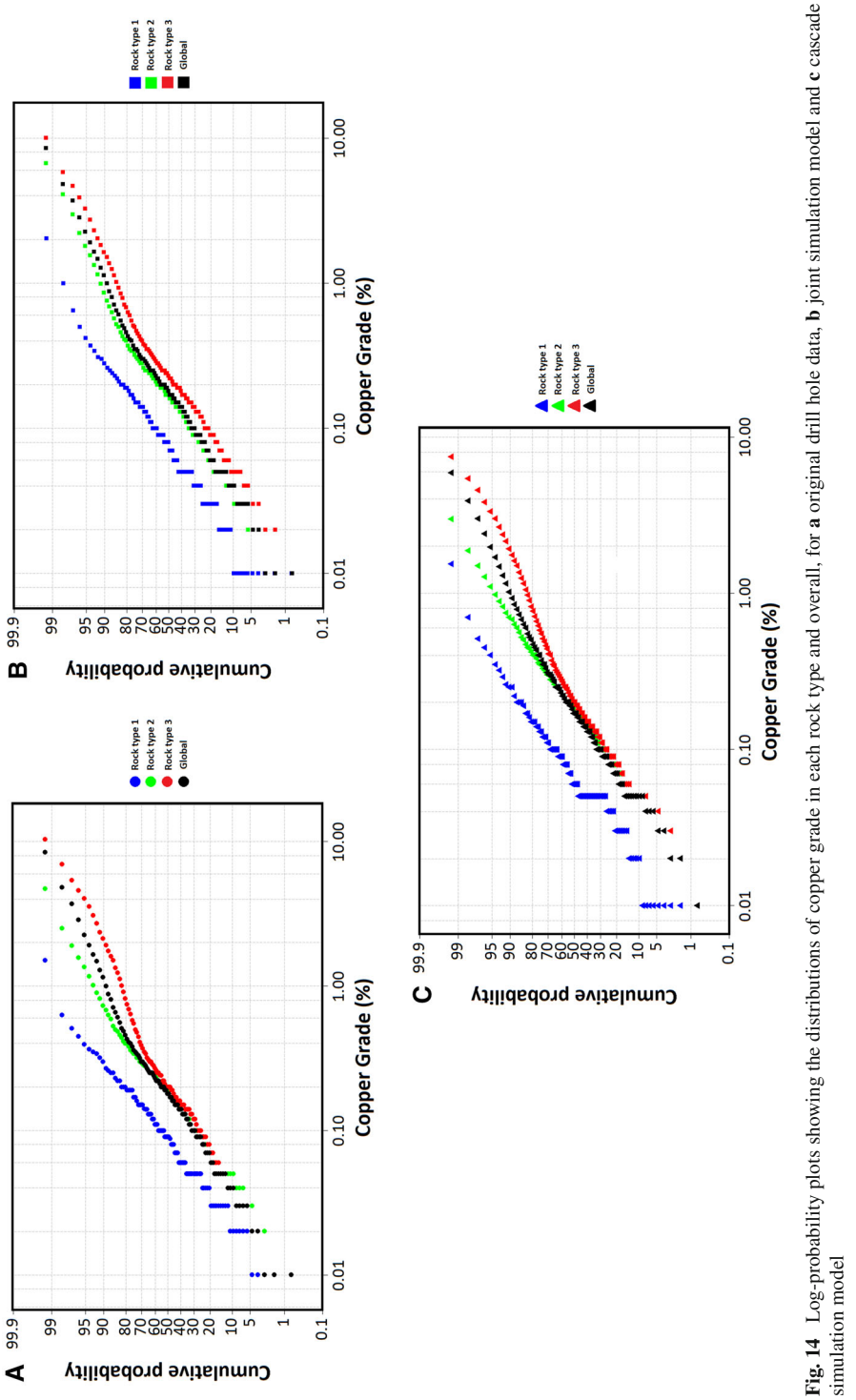

Fig. 14 Log-probability plots showing the distributions of copper grade in each rock type and overall, for **a** original drill hole data, **b** joint simulation model and **c** cascade simulation model

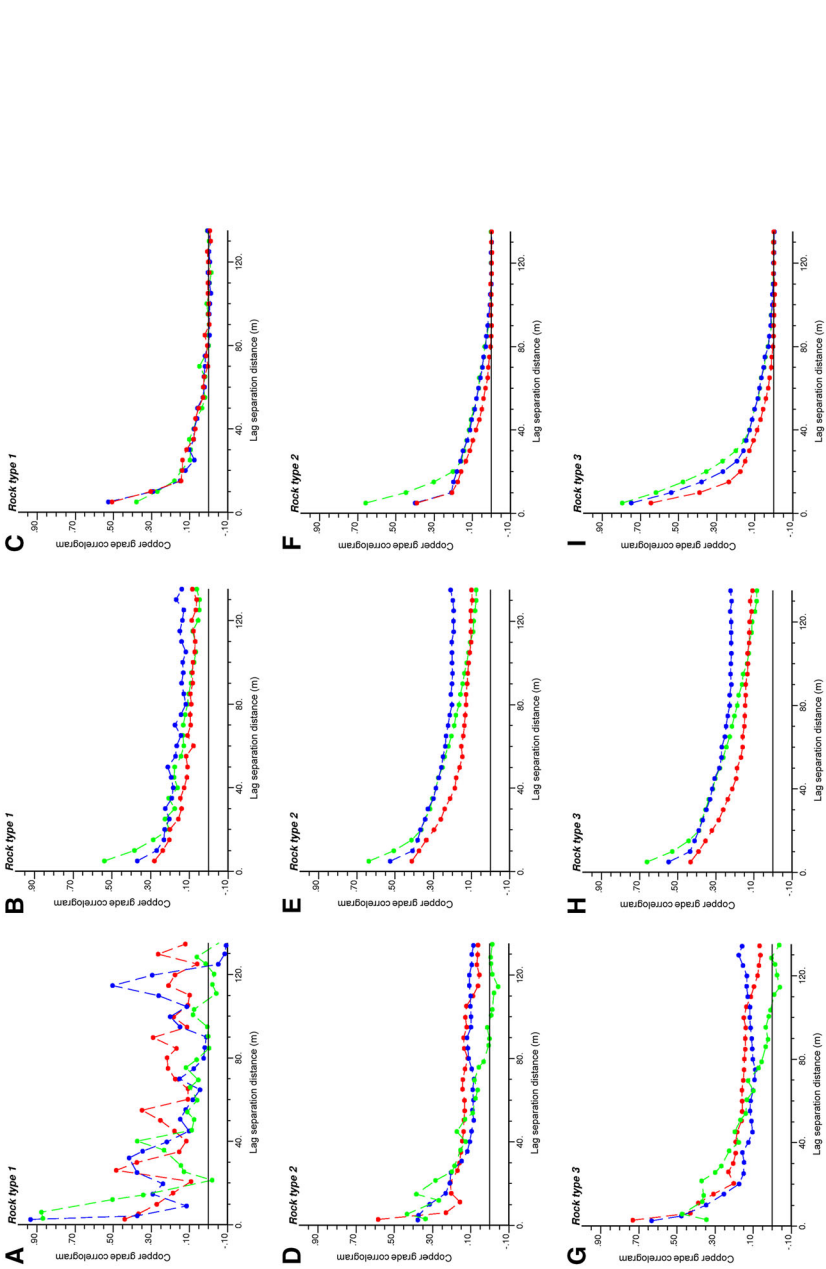

Fig. 15 Spatial correlation of copper grades within each rock type, calculated along main anisotropy directions (*green* N25°W, *red* N115°E dip −60°, *blue* N25°W dip −30°), for original data (**a**, **d**, **g**), joint simulation (**b**, **e**, **h**) and cascade simulation (**c**, **f**, **i**)

the simulated grades after separating by rock type. The resulting distributions prove to agree with the distributions observed on the data, within each rock type and overall (Fig. 14a, b). Concerning the cascade approach, as the copper grade is simulated within each rock type separately, the distribution in each rock type is also well reproduced when compared to the original data (Fig. 14a, c).

3.9.2 Spatial Correlation of Copper Grade Conditioned to Rock Type

In addition to marginal distributions, one can assess the spatial correlation of the simulated grade in each rock type and compare it with the experimental correlation observed in the data. It is seen (Fig. 15) that the correlation functions are generally well reproduced with both approaches (joint and cascade simulation), with a slightly better performance of one approach in some cases and of the other approach in other cases.

3.9.3 Rock-Type Boundaries

The differences between the two simulation approaches are more striking when looking at the behavior of the copper grade in the vicinity of a rock-type boundary. In particular, a look at the realizations indicates that the joint simulation tends to produce soft boundaries, with smooth transitions in the copper grade values (Fig. 10b, d), while the cascade simulation tends to produce hard boundaries, with abrupt changes in copper grade (Fig. 12b, d).

This is confirmed by examining the variations of mean grade when getting closer to a rock type boundary and by assessing the correlation of copper grade across a boundary, through mean graphs and correlation graphs similar to the ones used for contact analysis. Figures 16 and 17 show such graphs for the grades simulated with the two approaches. In the cascade approach, the mean grade shows an abrupt transition near the rock type boundaries (Fig. 16) and the simulated grades on either side of the boundaries are practically not correlated (Fig. 17). In contrast, with the joint simulation approach, the variations of mean grade are smoother and the simulated grades between both sides of the boundaries are correlated, as what is observed in the data (Fig. 4) (the more irregular profile of the data curves shown in Fig. 4 can be attributed to experimental fluctuations due to scarcity of data, rather than to a genuine behavior of the copper grade). The realizations obtained with the joint simulation approach are therefore more realistic in the neighborhood of rock-type boundaries and better suited to the description of the copper grade in the deposit.

4 Conclusions

Obtaining uncertainty models is a cumbersome process when one deals with regionalized variables of different natures that are cross-correlated, such as grades and rock types. In this study, two well-known geostatistical models are combined: the multiGaussian model to describe grades and the pluriGaussian model to describe rock types. The benefits of jointly simulating the grades and rock types with the proposed method

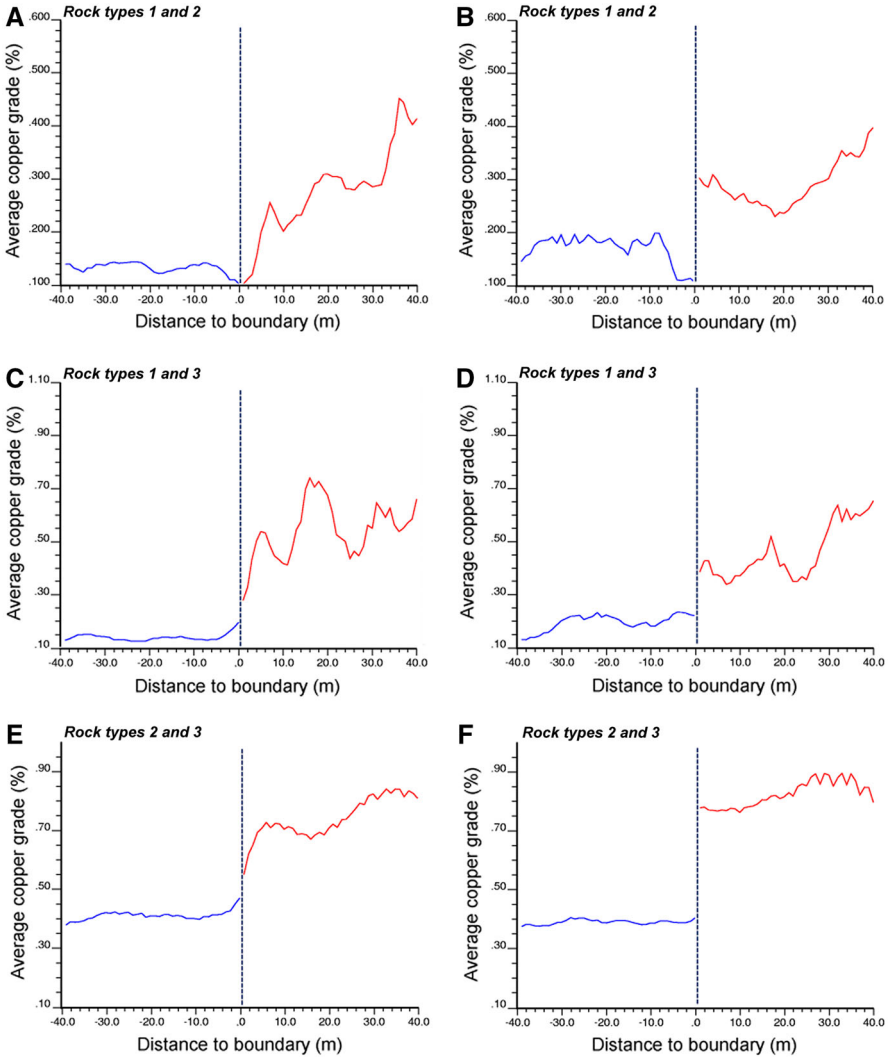

Fig. 16 Mean grade graphs for joint simulation (**a**, **c**, **e**) and cascade simulation (**b**, **d**, **f**)

are threefold. First, as opposed to deterministic rock-type modeling, one can measure the uncertainty in the rock-type layout, for example, through probability maps. Second, the spatial dependence between grade and rock type can be reproduced. Third, the spatial correlation of grade across rock-type boundaries is also reproduced, while this correlation is ignored using the cascade simulation approach.

The co-simulation approach is suitable when grades exhibit gradual transitions across rock-type boundaries. This happens in most ore deposits, in which there is no clear-cut discontinuity in the grade distribution when crossing a geological boundary, which can be explained because the physicochemical properties of the rock (pH,

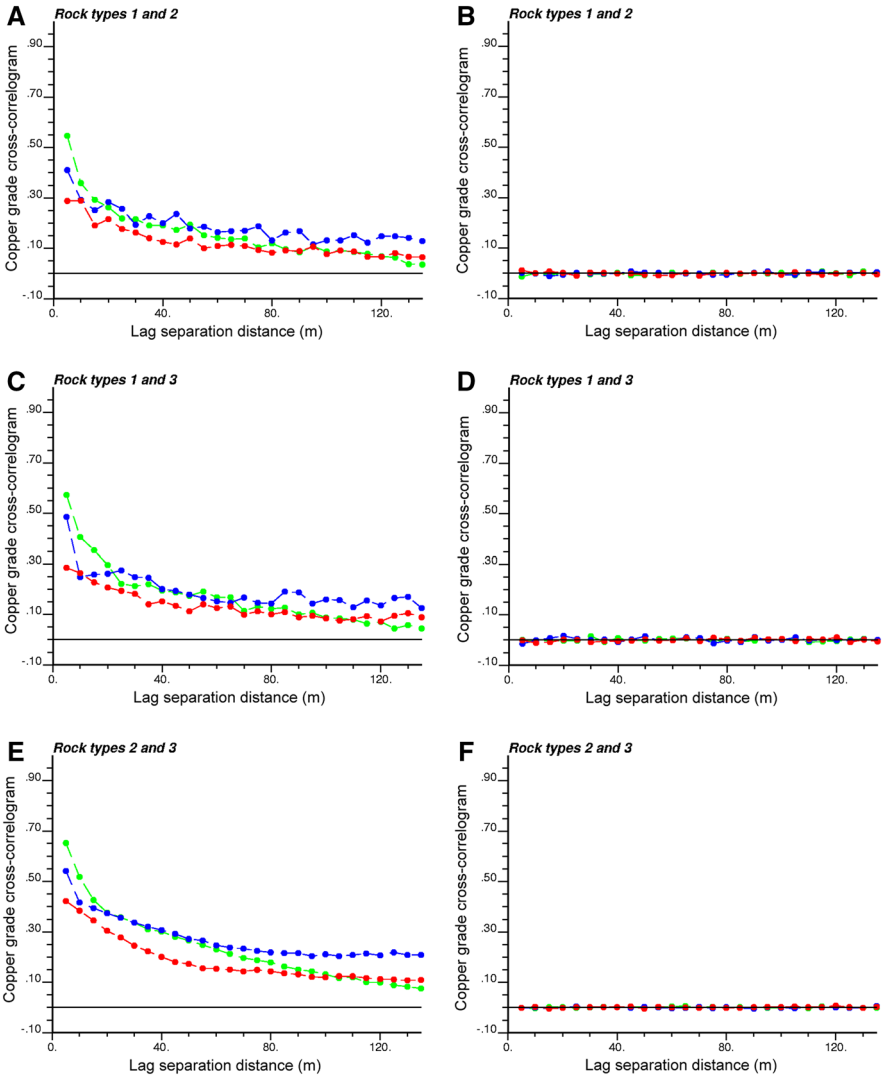

Fig. 17 Correlation graphs for joint simulation (**a**, **c**, **e**) and cascade simulation (**b**, **d**, **f**), calculated along main anisotropy directions (*green* N25°W, *red* N115°E dip −60°, *blue* N25°W dip −30°)

reduction potential, porosity, permeability, etc.) usually have transitional spatial variations. In contrast, the cascade approach consisting in simulating the rock types first, then the grades within each rock type, is adequate in the presence of hard boundaries. Such boundaries could be associated with faults or with geological gaps (vacuities or stratigraphic hiatii), among others.

Acknowledgments This research was funded by the Chilean Commission for Scientific and Technological Research, through Project CONICYT/FONDECYT/REGULAR/N° 1130085, and by a student research grant from the International Association for Mathematical Geosciences (Mathematical Geosciences Student

Award). The authors also acknowledge the support of Minera Michilla for providing the data set used in this work.

Appendix A: Relations Between Indicator Direct and Cross Variograms

In this study, three possible truncation rules that differ by the ordering of the rock types are under consideration (Fig. 6). A simple way to determine the most suitable truncation rule is to examine the direct and cross variograms of rock-type indicators (R_1, R_2 and R_3). In the model shown in Fig. 6a, the rock-type indicators are defined by truncating the Gaussian random fields Y_1 and Y_2 as follows

$$\begin{cases} R_1(\mathbf{x}) = 1_{Y_1(\mathbf{x})<y_1} \\ R_2(\mathbf{x}) = [1 - 1_{Y_1(\mathbf{x})<y_1}]\, 1_{Y_2(\mathbf{x})<y_2} \\ R_3(\mathbf{x}) = [1 - 1_{Y_1(\mathbf{x})<y_1}]\,[1 - 1_{Y_2(\mathbf{x})<y_2}]. \end{cases} \tag{6}$$

Let us calculate the cross variogram between R_1 and R_2 for a given lag separation vector $\mathbf{h}$

$$\begin{aligned} 2\gamma_{12}(\mathbf{h}) &= E\{[R_1(\mathbf{x}+\mathbf{h}) - R_1(\mathbf{x})]\,[R_2(\mathbf{x}+\mathbf{h}) - R_2(\mathbf{x})]\} \\ &= E\{[1_{Y_1(\mathbf{x}+\mathbf{h})<y_1} - 1_{Y_1(\mathbf{x})<y_1}]\,[1 - 1_{Y_1(\mathbf{x}+\mathbf{h})<y_1}]\, 1_{Y_2(\mathbf{x}+\mathbf{h})<y_2}\} \\ &\quad - E\{[1_{Y_1(\mathbf{x}+\mathbf{h})<y_1} - 1_{Y_1(\mathbf{x})<y_1}]\,[1 - 1_{Y_1(\mathbf{x})<y_1}]\, 1_{Y_2(\mathbf{x})<y_2}\}. \end{aligned} \tag{7}$$

Since Y_1 and Y_2 are independent, one obtains

$$\begin{aligned} 2\gamma_{12}(\mathbf{h}) &= E\{[1_{Y_1(\mathbf{x}+\mathbf{h})<y_1} - 1_{Y_1(\mathbf{x})<y_1}]\,[1 - 1_{Y_1(\mathbf{x}+\mathbf{h})<y_1}]\}\, E\{1_{Y_2(\mathbf{x}+\mathbf{h})<y_2}\} \\ &\quad - E\{[1_{Y_1(\mathbf{x}+\mathbf{h})<y_1} - 1_{Y_1(\mathbf{x})<y_1}]\,[1 - 1_{Y_1(\mathbf{x})<y_1}]\}\, E\{1_{Y_2(\mathbf{x})<y_2}\}. \end{aligned} \tag{8}$$

Because Y_2 is stationary, $E\{1_{Y_2(\mathbf{x}+\mathbf{h})<y_2}\} = E\{1_{Y_2(\mathbf{x})<y_2}\} = G(y_2)$, where G is the standard Gaussian cumulative distribution function. Therefore,

$$\begin{aligned} 2\gamma_{12}(\mathbf{h}) &= E\{[1_{Y_1(\mathbf{x}+\mathbf{h})<y_1} - 1_{Y_1(\mathbf{x})<y_1}]\,[1_{Y_1(\mathbf{x})<y_1} - 1_{Y_1(\mathbf{x}+\mathbf{h})<y_1}]\}\, G(y_2), \\ &= -2\, G(y_2)\, \gamma_{11}(\mathbf{h}), \end{aligned} \tag{9}$$

where $\gamma_{11}(\mathbf{h})$ is the direct variogram of R_1 for lag separation vector $\mathbf{h}$. Similarly, one finds that the cross variogram between R_1 and R_3 is proportional to γ_{11}

$$\gamma_{13}(\mathbf{h}) = [G(y_2) - 1]\, \gamma_{11}(\mathbf{h}). \tag{10}$$

Accordingly, the ratios of cross-to-direct variograms, $\gamma_{12}(\mathbf{h})/\gamma_{11}(\mathbf{h})$ and $\gamma_{13}(\mathbf{h})/\gamma_{11}(\mathbf{h})$, do not depend on $\mathbf{h}$. This property implies the absence of preferential contacts (edge effects) between rock type 1 and rock type 2, and between rock type 1 and rock type 3 (Rivoirard 1994; Séguret 2013).

The results concerning the flags shown in Fig. 6b, c are obtained by permuting the components of vector (R_1, R_2, R_3).

Appendix B: Distributions of Grade Conditional to Rock Type

In this appendix, it is of interest to determine, in the model fitted in Sects. 3.4–3.6, the distribution of grade conditional to the rock type, that is

$$\begin{aligned} G(y_0|\text{rock 1}) &= P\{Y_0(\mathbf{x}) < y_0 | Y_1(\mathbf{x}) < y_1\} \\ G(y_0|\text{rock 2}) &= P\{Y_0(\mathbf{x}) < y_0 | Y_1(\mathbf{x}) \geq y_1, Y_2(\mathbf{x}) < y_2\} \\ G(y_0|\text{rock 3}) &= P\{Y_0(\mathbf{x}) < y_0 | Y_1(\mathbf{x}) \geq y_1, Y_2(\mathbf{x}) \geq y_2\} \end{aligned} \tag{11}$$

for any real value y_0 (cut-off on the transformed copper grade).

To this end, let us expand the joint density of $\{Y_0(\mathbf{x}), Y_1(\mathbf{x})\}$ as follows (Lantuéjoul 2002)

$$g_{\rho_{01}}(y, y') = g(y)g(y') \sum_{p=0}^{+\infty} \frac{\rho_{01}^p}{p!} H_p(y) H_p(y'), \tag{12}$$

with g the standard Gaussian probability density function, ρ_{01} the correlation coefficient between $Y_0(\mathbf{x})$ and $Y_1(\mathbf{x})$, and H_p the Hermite polynomial of degree p, defined as

$$H_p(y) = \frac{1}{g(y)} \frac{\mathrm{d}^p g(y)}{\mathrm{d}y^p}. \tag{13}$$

By integrating term by term, one obtains the bivariate cumulative distribution function

$$\begin{aligned} G_{\rho_{01}}(y_0, y_1) &= \sum_{p=0}^{+\infty} \frac{\rho_{01}^p}{p!} \int_{-\infty}^{y_0} \int_{-\infty}^{y_1} g(y)g(y') H_p(y) H_p(y') \,\mathrm{d}y \,\mathrm{d}y' \\ &= G(y_0)G(y_1) + g(y_0)g(y_1) \sum_{p=1}^{+\infty} \frac{\rho_{01}^p}{p!} H_{p-1}(y_0) H_{p-1}(y_1). \end{aligned} \tag{14}$$

Likewise, the joint density of $\{Y_0(\mathbf{x}), Y_1(\mathbf{x}), Y_2(\mathbf{x})\}$ can be expanded as follows (Lantuéjoul 2002)

$$\begin{aligned} g_{\rho_{01},\rho_{02},\rho_{12}}(y, y', y'') = g(y)g(y')g(y'') \sum_{p,q,r=0}^{+\infty} \frac{\rho_{01}^p \rho_{02}^q \rho_{12}^r}{p!\,q!\,r!} \\ \times H_{p+q}(y) H_{p+r}(y') H_{q+r}(y''). \end{aligned} \tag{15}$$

A term-by-term integration leads to the trivariate cumulative distribution function

$$\begin{aligned} G_{\rho_{01},\rho_{02},\rho_{12}}(y_0, y_1, y_2) &= G(y_0)G(y_1)G(y_2) \\ &+ g(y_0)g(y_1) \sum_{p=0}^{+\infty} \frac{\rho_{01}^p}{p!} H_{p-1}(y_0) H_{p-1}(y_1) \end{aligned}$$

$$+g(y_0)g(y_2)\sum_{q=0}^{+\infty}\frac{\rho_{02}^{q}}{q!}\,H_{q-1}(y_0)\,H_{q-1}(y_2)$$
$$+g(y_1)g(y_2)\sum_{r=0}^{+\infty}\frac{\rho_{12}^{r}}{r!}\,H_{r-1}(y_1)\,H_{r-1}(y_2)$$
$$+\sum_{p,q,r=0}^{+\infty}\frac{\rho_{01}^{p}\,\rho_{02}^{q}\rho_{12}^{r}}{p\,!q!\,r!}\,g(y_0)g(y_1)g(y_2)\,H_{p+q-1}(y_0)\,H_{p+r-1}(y_1)\,H_{q+r-1}(y_2) \tag{16}$$

Accordingly, using the inclusion–exclusion principle, the distribution of grade conditional to the rock type [Eq. (11)] can be expressed as

$$G(y_0|\text{rock }1) = \frac{G_{\rho_{01}}(y_0, y_1)}{G(y_1)} \tag{17}$$
$$G(y_0|\text{rock }2) = \frac{G_{\rho_{02}}(y_0, y_2) - G_{\rho_{01},\rho_{02},\rho_{12}}(y_0, y_1, y_2)}{G(y_2) - G_{\rho_{12}}(y_1, y_2)} \tag{18}$$
$$G(y_0|\text{rock }3) = \frac{G(y_0) - G_{\rho_{01}}(y_0, y_1) - G_{\rho_{02}}(y_0, y_2) + G_{\rho_{01},\rho_{02},\rho_{12}}(y_0, y_1, y_2)}{1 - G(y_1) - G(y_2) + G_{\rho_{12}}(y_1, y_2)}. \tag{19}$$

References

Alabert FG, Massonnat GJ (1990) Heterogeneity in a complex turbiditic reservoir: stochastic modelling of facies and petrophysical variability. In: 65th annual technical conference and exhibition of the Society of Petroleum Engineers, SPE-20604, pp 775–790

Armstrong M, Galli A, Beucher H, Le Loc'h G, Renard D, Doligez B, Eschard R, Geffroy F (2011) Plurigaussian simulations in geosciences. Springer, Berlin

Boucher A, Dimitrakopoulos R (2012) Multivariate block-support simulation of the Yandi iron ore deposit, Western Australia. Math Geosci 44(4):449–468

Cáceres A, Emery X (2010) Conditional co-simulation of copper grades and lithofacies in the Rio Blanco-Los Bronces copper deposit. In: Castro R, Emery X, Kuyvenhoven R (eds) Proceedings of the IV international conference on mining innovation MININ 2010. Gecamin Ltd, Santiago, Chile, pp 311–320

Chilès JP, Delfiner P (2012) Geostatistics: modeling spatial uncertainty. Wiley, New York

Deutsch CV, Journel AG (1998) GSLIB: Geostatistical software library and user's guide. Oxford University Press, New York

Dowd PA, Pardo-Iguzquiza E, Xu C (2003) Plurigau: a computer program for simulating spatial facies using the truncated plurigaussian method. Comput Geosci 29(2):123–141

Duke JH, Hanna PJ (2001) Geological interpretation for resource modelling and estimation. In: Edwards AC (ed) Mineral resource and ore reserve estimation—the AusIMM guide to good practice. The Australasian Institute of Mining and Metallurgy, Melbourne, pp 147–156

Emery X (2007) Simulation of geological domains using the plurigaussian model: new developments and computer programs. Comput Geosci 33(9):1189–1201

Emery X (2008) A turning bands program for conditional co-simulation of cross-correlated Gaussian random fields. Comput Geosci 34(12):1850–1862

Emery X, Lantuéjoul (2006) TBSIM: a computer program for conditional simulation of three-dimensional Gaussian random fields via the turning bands method. Comput Geosci 32(10):1615–1628

Emery X, Silva DA (2009) Conditional co-simulation of continuous and categorical variables for geostatistical applications. Comput Geosci 35(6):1234–1246

Glacken IM, Snowden DV (2001) Mineral resource estimation. In: Edwards AC (ed) Mineral resource and ore reserve estimation—the AusIMM guide to good practice. The Australasian Institute of Mining and Metallurgy, Melbourne, pp 189–198

Jones P, Douglas I, Jewbali A (2013) Modeling combined geological and grade uncertainty: application of multiple-point simulation at the Apensu gold deposit, Ghana. Math Geosci 45(8):949–965

Journel AG, Alabert FG (1990) New method for reservoir mapping. J Pet Technol 42(2):212–218

Journel AG, Huijbregts CJ (1978) Mining geostatistics. Academic Press, London

Kim HM, Mallick BK, Holmes CC (2005) Analyzing nonstationary spatial data using piecewise Gaussian processes. J Am Stat Assoc 100(470):653–668

Lantuéjoul C (2002) Geostatistical simulation: models and algorithms. Springer, Berlin

Larrondo P, Leuangthong O, Deutsch CV (2004) Grade estimation in multiple rock types using a linear model of coregionalization for soft boundaries. In: Magri E, Ortiz J, Knights P, Henríquez F, Vera M, Barahona C (eds) Proceedings of the 1st international conference on mining innovation. Gecamin Ltd, Santiago, Chile, pp 187–196

Mackenzie DH, Wilson GI (2001) Geological interpretation and geological modeling. In: Edwards AC (ed) Mineral resource and ore reserve estimation—the AusIMM guide to good practice. The Australasian Institute of Mining and Metallurgy, Melbourne, pp 111–118

Oliveros V, Trsitá-Aguilera D, Féraud G, Morata D, Aguirre L, Kojima S, Ferraris F (2008) Time relationships between volcanism–plutonism–alteration–mineralization in Cu-stratabound ore deposits from the Michilla mining district, northern Chile: a 40Ar/39Ar geochronological approach. Miner Depos 43(1):61–78

Ortiz JM, Emery X (2006) Geostatistical estimation of mineral resources with soft geological boundaries: a comparative study. J S Afr Inst Min Metall 106(8):577–584

Rivoirard J (1994) Introduction to disjunctive kriging and non-linear geostatistics. Oxford University Press, Oxford

Roldão D, Ribeiro D, Cunha E, Noronha R, Madsen A, Masetti L (2012) Combined use of lithological and grade simulations for risk analysis in iron ore, Brazil. In: Abrahamsen P, Hauge R, Kolbjørnsen O (eds) Geostatistics Oslo 2012. Springer, Berlin, pp 423–434

Rossi ME, Deutsch CV (2014) Mineral resource estimation. Springer, Dordrecht

Séguret SA (2013) Analysis and estimation of multi-unit deposits: application to a porphyry copper deposit. Math Geosci 45(8):927–947

Strebelle S (2002) Conditional simulation of complex geological structures using multiple-point statistics. Math Geol 34(1):1–22

Vargas-Guzmán JA (2008) Transitive geostatistics for stepwise modeling across boundaries between rock regions. Math Geosci 40(8):861–873

Wackernagel H (2003) Multivariate geostatistics: an introduction with applications. Springer, Berlin

Wilde BJ, Deutsch CV (2012) Kriging and simulation in presence of stationary domains: developments in boundary modeling. In: Abrahamsen P, Hauge R, Kolbjørnsen O (eds) Geostatistics Oslo 2012. Springer, Berlin, pp 289–300